

# HIGH CAPTURE LOW ENERGY SPREAD INVERSE FREE ELECTRON LASER ACCELERATOR

J. P. Duris, R. K. Li, P. Musumeci, E. Threlkeld

Department of Physics and Astronomy, UCLA, Los Angeles, CA 90095, USA

## Abstract

We present the design and construction of a strongly period-, field-, and gap-tapered helical undulator for use in a high-gradient, high-efficiency helical IFEL experiment at Brookhaven ATF. The undulator design achieves efficient acceleration without prebunching by matching the ponderomotive and resonant energy gradients along the length of the interaction for the measured laser parameters. Simulations based on the measured undulator fields and experimental parameters suggest that as much as 43% of a 50 MeV beam will be accelerated to 94 MeV with 2.3% rms energy spread.

## INTRODUCTION

Recent progress in inverse free electron laser acceleration (IFEL) has led to unprecedented acceleration gradients and energy gain for this class of accelerator. The STELLA experiment at ATF demonstrated efficient IFEL acceleration with gradients similar to conventional RF-accelerating cavities and captured up to 80% of the beam with the use of a prebunched beam [1]. The UCLA Neptune IFEL experiment first achieved accelerating gradients surpassing that of conventional rf-accelerators [2]. More recently, the UCLA-BNL helical IFEL collaboration at the Brookhaven Accelerator Test Facility (ATF) accelerated electrons from 52 MeV up to 106 MeV with a TW class CO<sub>2</sub> laser, averaging a 100 MeV/m accelerating gradient in the 54 cm long helical undulator [3]. The LLNL-UCLA IFEL effort currently underway at Lawrence Livermore National Lab aims to surpass these achievements by utilizing a multi-TW Ti:Sa laser [4] and has produced some significant initial results [5].

While IFEL accelerating gradients now outpace that of their rf counterparts, the higher gradients often come at the price of significant energy spread and low capture. One approach to improving capture is to match the longitudinal phase space of the beam to the longitudinal acceptance of the accelerator through microbunching as demonstrated by [1], and novel optical scale harmonic and adiabatic bunchers hold the promise of improved microbunching [6]. However, the efficiency of IFEL accelerators is often limited by spatiotemporal overlap of electron and laser beams as well as resonant energy and ponderomotive gradient mismatch. We aim to address these issues to allow monoenergetic acceleration with gradients larger than that of conventional accelerators without the use of prebunching.

02 Light Sources

A15 - New Acceleration Techniques

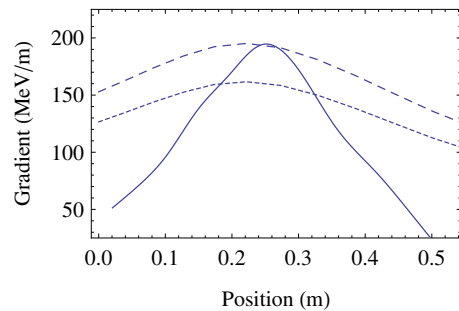


Figure 1: Resonant energy gradient set by the undulator tapering (solid) and ponderomotive gradients for the highest laser focal intensity of 23 TW/cm<sup>2</sup> (dashed) as well as for the median intensity of 18 TW/cm<sup>2</sup> (dotted).

## GRADIENT MISMATCH

The UCLA-BNL helical IFEL collaboration at ATF was conceived to improve accelerating gradient through the use of the first strongly period- and field-tapered helical undulator. Whereas electrons propagating through a linear undulator undergo sinusoidal motion thereby reducing to zero twice per period their transverse velocity, the helical trajectories of the electrons propagating through the undulator provide continuous transverse velocity which in turn enables continuous energy transfer. This, coupled with a TW-class CO<sub>2</sub> laser, allowed for the acceleration of 52 MeV electrons up to 106 MeV [3].

The undulator was originally designed for use with a 9.6 cm Rayleigh range CO<sub>2</sub> laser. Unfortunately after construction, it was discovered that beam line space constraints and a restricting dipole aperture just upstream of the undulator necessitated a laser Rayleigh range of 30 cm. While the increased Rayleigh range had the positive benefit of easing transverse overlap tolerances by increasing the laser spot size, the on-axis intensity was reduced 3-fold, thereby significantly limiting the fraction captured and challenging the success of the experiment.

The problem can be better visualized by comparing the gradients set by the tapering of the undulator and that supplied by the ponderomotive interaction of the electrons in the combined undulator- and laser-fields. Figure 1 shows the resonant energy gradient set by the undulator and the ponderomotive gradient for various focal laser intensities (right plot). The resonant energy gradient usually exceeded the ponderomotive gradient, thereby significantly increasing the number of particles lost by reducing the ponderomotive bucket depth.

ISBN 978-3-95450-138-0

619

## HELICAL UNDULATOR

In order to improve the efficiency of the interaction, either the laser focusing must be changed to match the undulator design or the undulator tapering must be modified to match the laser. The former proved to be expensive as the dipole gap would have to be increased and impractical since due to the experimental hall layout, the focusing optics would have to be placed in the middle of a walkway, blocking access to vacuum equipment and interlock systems. The chosen solution was to redesign and rebuild the undulator to accommodate the more relaxed laser focusing.

The helical undulator is the superposition of two Halbach permanent magnet undulators rotated 90 degrees about their common axis and shifted in phase by a quarter wavelength [7]. Each of the four opposing pairs of NdFeB magnets per period determines the period and on-axis field of each undulator for a fixed gap of 15 mm. In order to relax the tapering, we tapered the gap of the undulator. This extra degree of freedom enabled us to change the undulator strength  $K$  while the period remained fixed.

### Undulator Design

The undulator design follows closely the methods described in [8]. Equations 1 and 2 describe the approximate longitudinal dynamics of a particle undergoing helical IFEL interaction. Here,  $K_l = \frac{eE_0\lambda}{m_0c^22\pi}$  and  $K = \frac{eB\lambda_w}{m_0c^22\pi}$  are the laser and undulator normalized vector potentials respectively.

$$\frac{d\gamma}{dz} = \frac{kK_lK}{\gamma} \sin \psi \quad (1)$$

$$\frac{d\psi}{dz} = k_w - k \frac{1 + K^2}{2\gamma^2} \quad (2)$$

Equation 1 describes the ponderomotive gradient due to the combined interaction of undulator- and laser-fields as evident by the presence of  $K$  and  $K_l$  in the equation. For a stationary resonant phase, a resonant particle's energy is determined completely by setting the phase advance to zero in Equation 2, thereby yielding the energy of the resonant particle:  $\gamma_r = \sqrt{\frac{\lambda_w}{2\lambda} (1 + K^2)}$ . This resonant energy depends only on the undulator field strength  $K$  and wavelength  $\lambda_w$ ; therefore, the gradient in the resonant energy is determined completely by the undulator.

The undulator tapering is then determined by Equation 3 which is found by equating the ponderomotive gradient from Equation 1 with the gradient in the resonant energy set by the undulator tapering. When the undulator period and laser parameters are specified along with the initial condition that  $K$  at the entrance be such that the resonant energy is equal to the input beam's 50 MeV, the differential equation yields  $K$  which in turn determines the on-axis field strength along the undulator. The undulator builder equation can then be used to estimate the gap along the undulator needed to create the designed on-axis field. The measured laser and e-beam parameters used in the tapering

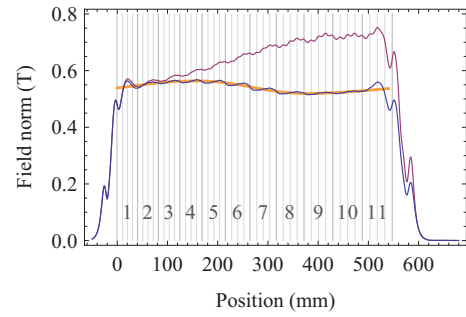


Figure 2: Design magnetic field amplitude along the undulator (orange) along with Radia simulation (blue) and the previous constant-gap undulator field (purple).

design are specified in Table 1. The design laser focal intensity dictates the threshold for full acceleration and was set to be 4 TW/cm<sup>2</sup> in order to be well within the capabilities of the laser in order to achieve full acceleration for most shots; furthermore, simulations show that this choice of design intensity maximizes capture for the more typical intensity of 18 TW/cm<sup>2</sup> observed previously. The resonant phase was chosen to be a constant  $\pi/4$  as a compromise between bucket depth and ponderomotive gradient.

$$\frac{dK}{dz} = \frac{8\pi K K_l \sin \psi_r - \frac{d\lambda_w}{dz} (1 + K^2)}{2\lambda_w K} \quad (3)$$

Table 1: Design Parameters

E-beam energy	50 MeV
Laser focal intensity	4 TW/cm <sup>2</sup>
Laser wavelength	10.3 $\mu$ m
Rayleigh range	30 cm
1/e <sup>2</sup> spot size	0.99 mm
M <sup>2</sup>	1.07
Resonant phase	$\pi/4$
Laser waist	undulator midpoint

The 3D magnetostatic field solver Radia [9] was used to determine the placement of each magnet. Figure 2 shows the design field determined by the differential equation for  $K$  discussed above along with the field simulated by Radia with the design magnet gap configuration. The ripple in the Radia simulated field was introduced to minimize trajectory deflections for particles propagating on axis through the undulator. The trajectory is determined by the second integral of the field; however as the field increases towards the end of each period, the integral over one period is non-zero and the net effect is a kick to the particles. The ripple minimizes this deflection by canceling the second integral over each period.

### Construction and Measurement

The undulator magnets are held in place by bolts which provide fine tuning of the gap over a range of a couple mm;

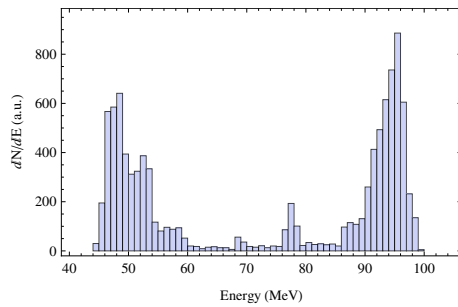


Figure 3: TREDI simulation utilizing the measured fields.

however since the half gap needed to be increased by about 2.5 mm towards the undulator's exit, aluminum shims were introduced to increase it by 3 mm. Measurements of the height of each magnet, width of the rails for each period, and the overall shim distance allowed for an estimate of the initial half gap with magnets retracted fully. The difference between design and measured half gap was calculated, and each magnet was driven into place. Since thread tolerances cause up to 200  $\mu\text{m}$  play as each bolt was turned, a hall sensor was positioned on axis near each magnet before moving to detect movement as its corresponding bolt was turned.

After the initial magnet placement, the on-axis fields were measured and found to be systematically low by a couple percent. Magnets were then tuned slightly in pairs to increase the field to that of the Radia simulations. Finally, the fields were finely tuned to reduce the transverse kick and offset estimated by the first and second integrals of the field for a beam with energy 50 MeV. The final measured fields were found to agree to within 0.5% rms of the Radia simulations.

## SIMULATIONS

Simulations were performed with the 3D IFEL code TREDI and are shown in Figure 3 for a 50 MeV input e-beam, laser focusing parameters listed in Table 1, and 18  $\text{TW}/\text{cm}^2$  laser focal intensity. TREDI solves the Lorentz force equations rather than averaging the motion of the electrons over an undulator period [10] and was previously bench-marked against IFEL experimental results in planar undulators [2]. The simulation includes time dependent effects, and the 1 ps long e-beam and 4.5 ps laser pulse are synchronized at the entrance to the undulator. The simulations show that for the expected experimental parameters, up to 43% of the beam is captured and transported to greater than 90 MeV. The accelerated beam has a mean energy of 94 MeV, energy spread of 2.3%, and is microbunched at 10.3  $\mu\text{m}$ .

One of the benefits of the relaxed tapering is the relatively modest requirements on the laser performance. Figure 4 shows how the maximum particle energy varies as the input laser focal intensity is increased. While the laser focal intensity was previously seen to usually exceed 15  $\text{TW}/\text{m}^2$ , the threshold for acceleration to 90 MeV for the measured undulator is just 5  $\text{TW}/\text{cm}^2$ . This suggests that

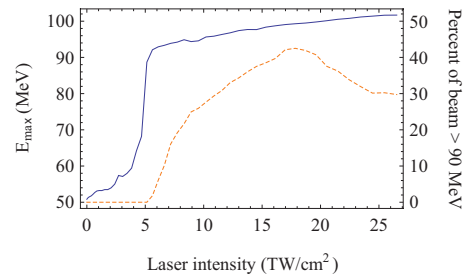


Figure 4: Maximum particle energy (solid) and fraction of beam with energy greater than 90 MeV (dashed) as a function of input laser focal intensity.

full energy acceleration should be obtained for most shots. Furthermore, a quarter of the beam is accelerated to greater than 90 MeV when the intensity is doubled to 10  $\text{TW}/\text{cm}^2$ . These modest requirements on laser intensity for full acceleration open the door to studies of the accelerated beam.

## CONCLUSIONS

While recent achievements in IFEL acceleration have focused on either high gradient or high efficiency acceleration, the UCLA-BNL helical IFEL collaboration aims to achieve both without the need for prebunching. The undulator tapering design achieves this by matching the resonant energy and ponderomotive accelerating gradients using the measured laser parameters through the novel strongly period-, field-, and gap-tapered helical undulator. The laser focal intensity threshold for full acceleration is well within the laser's observed limits leading to the possibility of studies of the accelerated beam. For moderate laser intensities, up to 43% of the e-beam should be transported to full energy, and production of a monoenergetic beam with few percent energy spread is expected.

This work was supported by DOE grant DE-FG02-92ER40693, Defense of Threat Reduction Agency award HDTRA1-10-1-0073 and University of California Office of the President award 09-LR-04-117055-MUSP.

## REFERENCES

- [1] W. Kimura et al., *Phys. Rev. Lett.*, 92:054801, 2004.
- [2] P. Musumeci et al., *Phys. Rev. Lett.*, 94:154801, 2005.
- [3] J. Duris et al. Submitted to *Phys. Rev. Lett.*
- [4] J. Moody et al. in Proceedings of the 2012 International Particle Accelerator Conference, New Orleans, LA, 2012.
- [5] J. Moody et al., MOPAC43, NA-PAC'13.
- [6] L. Ho et al., TUPAC29, NA-PAC'13.
- [7] J. Duris et al. in Proceedings of the 2012 International Particle Accelerator Conference, New Orleans, LA, 2012.
- [8] J. Duris, P. Musumeci, R. Li. *Phys. Rev. ST Accel. Beams*, 15:061301, 2012.
- [9] O. Chubar, P. Elleaume and J. Chavanne. *J. Synchrotron Rad.*, 5, 481- 484, 1998.
- [10] L. Giannessi, P. Musumeci, M. Quattromini *Nucl. Instrum. Methods Phys. Res., Sect. A*, 436, 443, 1999.